ACS OMEGA

Open Access



http://pubs.acs.org/journal/acsodf

Article

# Facile Preparation of Magnetic $CuFe_2O_4$ on Sepiolite/GO Nanocomposites for Efficient Removal of Pb(II) and Cd(II) from Aqueous Solution

Israa Othman, Fawzi Banat, Shadi W. Hasan, Cyril Aubry, Sundaramurthy Suresh, Mika Sillanpää, and Mohammad Abu Haija*

Cite This: *ACS Omega* 2023, 8, 38828−38838

Read Online

ACCESS | Metrics & More | Article Recommendations

**ABSTRACT:** $CuFe_2O_4$ nanoparticles were synthesized and immobilized on sepiolite fibers and graphene oxide sheets, producing a $CuFe_2O_4$/sepiolite/GO (CFSG) nanocomposite via a facile single-pot method. The synthesized nanocomposite was characterized using TEM, FTIR, SEM−EDX, XRD, and TGA techniques to determine its composition, structure, and thermal stability. The adsorptive removal of Pb(II) and Cd(II) heavy metal ions from aqueous solutions was studied using the synthesized CFSG nanocomposite. Adsorption parameters such as CFSG loading, pH, contact time, and temperature were investigated. The CFGS nanocomposite showed a higher Pb(II) removal ($q_m$ = 238.1 mg/g) compared to Cd(II) ($q_m$ = 14.97 mg/g) in a Pb(II) and Cd(II) binary system. The Pb(II) and Cd(II) adsorption fitted well with the Langmuir model, followed by the pseudo-second-order model, and was found spontaneous. Adsorption thermodynamic analysis showed that the Pb(II) adsorption process was exothermic while Cd(II) adsorption was endothermic. The $CuFe_2O_4$ nanoparticles on the CFSG surface could facilitate the adsorption of heavy metal ions through electrostatic interaction and complexation processes.

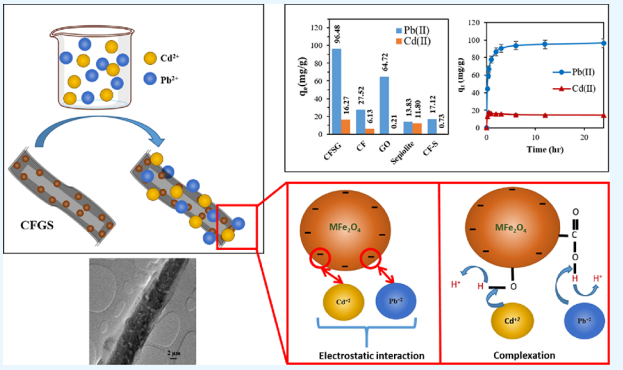


## 1. INTRODUCTION

Discharged industrial effluents contain different types of contaminants that can be toxic and pose a serious threat to human health and ecosystem. Such contaminants include organic and inorganic compounds, heavy metals, pharmaceuticals, and pigments.[1] Heavy metals are often present in discharged wastewater from different industries, such as textiles, oil processing, photography, and steel planting facilities.[2,3] As two of the most common toxic heavy metals, both lead (Pb(II)) and cadmium (Cd(II)) can cause severe problems in humans such as blood disorders, kidney failure, depression, osteoporosis, mental disorders, and cancers.[1,4] According to the World Health Organization (WHO) and the US Environmental Protection Agency (EPA), the highest permitted levels for Pb(II) and Cd(II) in drinking water are 0.01 and 0.005 mg/L, respectively.[5] Therefore, it is essential to remove them from the wastewater before discharging it into the environment.

Different methods were reported for heavy metals wastewater treatment, including adsorption,[6−8] membrane technology,[2] flotation,[1] and ion exchange.[4] Some of these methods had significant drawbacks, such as the production of sludge, high cost, or limited operational conditions. In contrast, the adsorption method seems to be one of the most practical choices because of its feasibility, low cost, and simple operation.[9,10] Thus, the synthesis of an adsorbent with a high affinity toward heavy metals removal was vastly investigated.[7,11] Many kinds of adsorbents, including carbon-based composites, activated carbon, nanoparticles, and clays, are used to remove heavy metals from wastewater.[7,9,10]

Copper ferrite nanoparticles ($CuFe_2O_4$ NPs) are metal oxides with distinctive physicochemical, optical, and magnetic properties that allow them to be used in various applications, such as catalysis,[12] gas sensors,[13,14] membrane fabrication,[15] and capacitive deionization.[16] However, $CuFe_2O_4$ NPs tend to agglomerate due to their magnetic properties, which reduces their surface areas and the exposed adsorption active sites. This

Received: March 25, 2023
Accepted: July 25, 2023
Published: October 12, 2023

issue can be resolved using carbon-based or silica-based materials as supports for $CuFe_2O_4$ NPs.[17,18]

Sepiolite is a natural silicate clay mineral that exists in the form of microfibers.[19] It is a potential support for NPs due to its high surface area, and mechanical and chemical stability.[20] Several reports showed that clays exhibit high heavy metals removal.[21,22] Graphene oxide (GO) is also a commonly used support for NPs due to its high surface area and surface properties.[18] Therefore, the use of GO as a support is expected to improve the dispersion of NPs and the adsorption performance.[23] Ferrite/GO composites were used to remove heavy metals from water. For instance, the $MnFe_2O_4$/GO composite was studied for the adsorption of methylene blue dye and arsenic(V) ions[24] and $NiFe_2O_4$/GO and $CoFe_2O_4$/GO composites were reported for Pb(II) and Cd(II) adsorption.[25] Furthermore, the bentonite/$CoFe_2O_4$/hydroxyapatite composite was investigated for Pb(II) adsorption.[2]

In this study, a $CuFe_2O_4$/sepiolite/GO (CFSG) nanocomposite was prepared and investigated as an adsorbent for the removal of toxic pollutants from water. The novelty of the work lies in the nanocomposite and its application for the simultaneous removal of Pb(II) and Cd(II) from aqueous solutions. The synthesized ternary nanocomposite has not been reported before—only related binary nanocomposites, such as ferrite/GO and ferrite/clay nanocomposites—have been reported. The adsorptive removal of Cd(II) and Pb(II) binary systems by the CFSG nanocomposite was investigated using batch adsorption experiments. The kinetics, isotherms, and thermodynamic parameters of adsorption were evaluated. Moreover, the effects of CFSG loading, pH, contact time, and temperature on the adsorption process were investigated.

## 2. EXPERIMENTAL SECTION

**2.1. Chemicals.** All chemicals used in this research were of analytical grade and utilized without further purification. Graphite flakes were obtained from Asbury Carbons. Ferric nitrate ($Fe(NO_3)_3{\cdot}9H_2O$), hydrochloric acid (HCl, 37%, solution), and hydrogen peroxide ($H_2O_2$, 30% solution) were purchased from Merck. Ammonium hydroxide ($NH_4OH$, 30% solution), sulfuric acid ($H_2SO_4 \approx$ 98% solution), sodium hydroxide (NaOH, 99.7%), and phosphoric acid ($H_3PO_4$, 85% solution) were supplied by BDH. Lead(II) nitrate ($Pb(NO_3)_2$) was provided by Schalau. Citric acid, cadmium chloride ($CdCl_2{\cdot}2.5H_2O$), copper(II) chloride ($CuCl_2{\cdot}2H_2O$), and sepiolite were obtained from Sigma-Aldrich.

**2.2. Synthesis of GO.** GO was prepared using a modified Hummer method,[26] in which 10 g of graphite flakes was dispersed in 560 mL of $H_2SO_4$ and 66 mL of $H_3PO_4$ under continuous stirring for 30 min. Then, 56 g of $KMnO_4$ was slowly added to the mixture and stirred for 3 days. 75 mL of 30% $H_2O_2$ was mixed with 250 mL of deionized (DI) water and then slowly added to the mixture under continuous stirring for 4 h. Finally, a dark-brown slurry was collected using centrifugation and the product was separated and washed with 2 M HCl, DI water, and ethanol.

**2.3. Synthesis of $CuFe_2O_4$/Sepiolite/GO Nanocomposites.** The nanocomposite was prepared using a co-precipitation method as follows: 0.25 g of GO and 1 g of sepiolite were dispersed in water for 1 h. Then, pre-determined quantities of $CuCl_2{\cdot}2H_2O$ and $Fe(NO_3)_2{\cdot}9H_2O$, with a molar ratio of 1:2, respectively, were dissolved separately in DI water.[27] The two solutions were mixed and heated at 60 °C for 30 min, and subsequently, the pH was adjusted to 12 using 5 M NaOH. Finally, the obtained product was collected, washed, and dried in an oven at 100 °C. The final product (CFGS) was ground and stored.

**2.4. Characterization.** FTIR measurements were performed in the range of 400−4000 $cm^{-1}$ using a Bruker Alpha Platinum ATR spectrometer. The surface morphological and elemental properties of the nanocomposite were investigated by SEM using FEI Quanta 250 coupled with an EDAX Apollo SDD detector. TEM analysis was carried out at 300 kV using a Titan electron microscope. XRD measurements were performed using Bruker D2 PHASER XRD with Cu K$\alpha$ radiation at 1.54 Å, 30 kV, and 10 mA, in the range of 2$\theta$ from the 10 to 80° range with a step size of 0.02°. With a Perkin Elmer 6000, thermogravimetric analysis was carried out to investigate the thermal stability of the nanocomposite from 30 to 700 °C at a heating rate of 10 °C/min under nitrogen flow.

**2.5. Adsorption Batch Experiments.** Stock solutions were prepared by dissolving 100 mg of $Pb(NO_3)_2$ and 100 mg of $CdCl_2{\bullet}2.5H_2O$ in 1 L of DI water. Batch experiments were carried out using 25 mL Erlenmeyer flasks containing 10 mL of 100 mg/L Cd(II) and 100 mg/L Pb(II), to which 10 mg of CFSG composite was added. The adsorption experiments were run in three replicates. The effects of experimental parameters, including adsorbent dosage, pH, contact time, and temperature, on the adsorption process were investigated.

## 3. RESULTS AND DISCUSSION

**3.1. CFSG Characterization.** FTIR analyses were conducted in a range of 400−4000 $cm^{-1}$, and the obtained spectra are presented in Figure 1. The characteristic peaks of

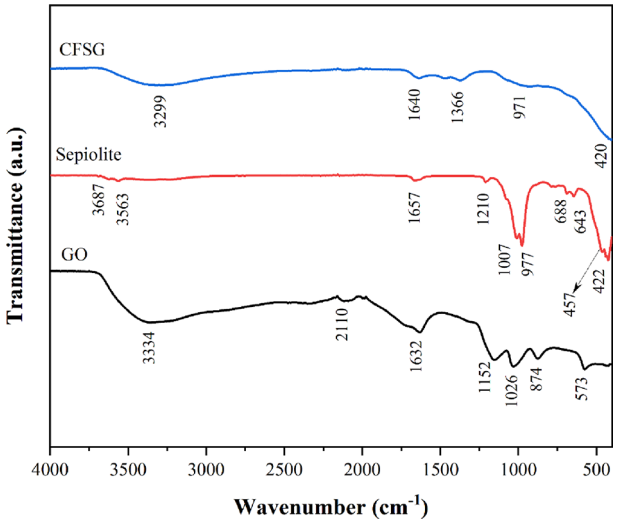


**Figure 1.** FTIR spectra of GO, sepiolite, and CFSG.

the GO were observed at 3334, 1716, 1632, 1152, and 1026 $cm^{-1}$, corresponding to O−H, C═O, C═C, C−OH, and C−O, respectively.[18,24,28] The sepiolite IR spectrum showed peaks at 3687 $cm^{-1}$ attributed to Mg−OH stretching vibration and at 3563 and 1657 $cm^{-1}$ due to coordinated water stretching bands.[20] The two peaks at 688 and 643 corresponded to the Mg−OH bending vibrations.[22] The peaks at 788, 457, and 422 $cm^{-1}$ can be related to the O−H bond bending of Mg−Fe−OH, Si−O−Si bending vibration, and Si−O−Mg octahedral−tetrahedral bond vibration, respectively.[19,20,22] Furthermore, sepiolite showed absorption bands at 1210 and 977 $cm^{-1}$


https://doi.org/10.1021/acsomega.3c02006
ACS Omega 2023, 8, 38828−38838

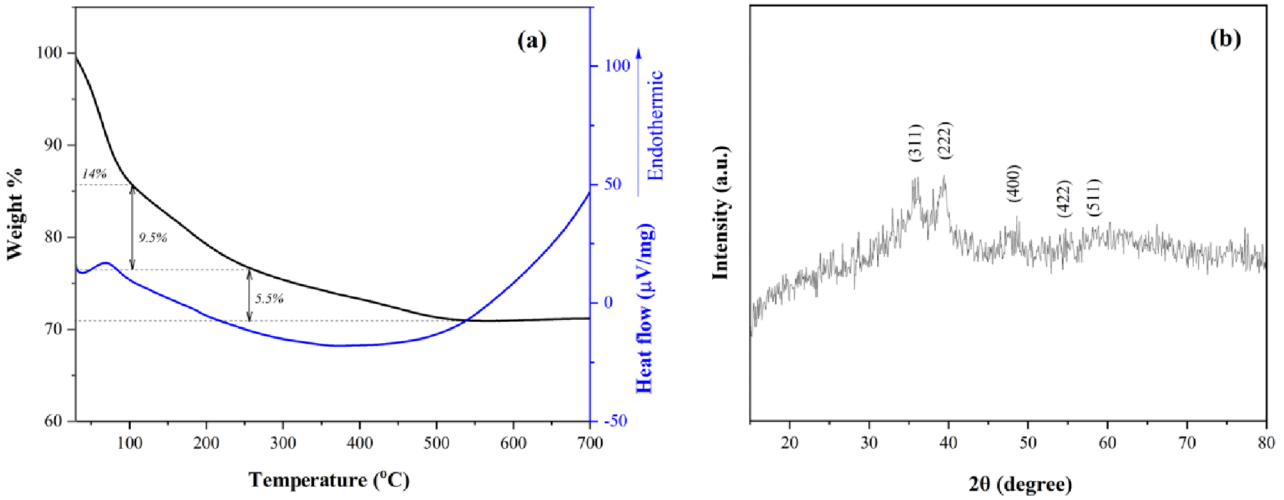


**Figure 2.** (a) TGA and DTA curves and (b) XRD pattern of CFSG.

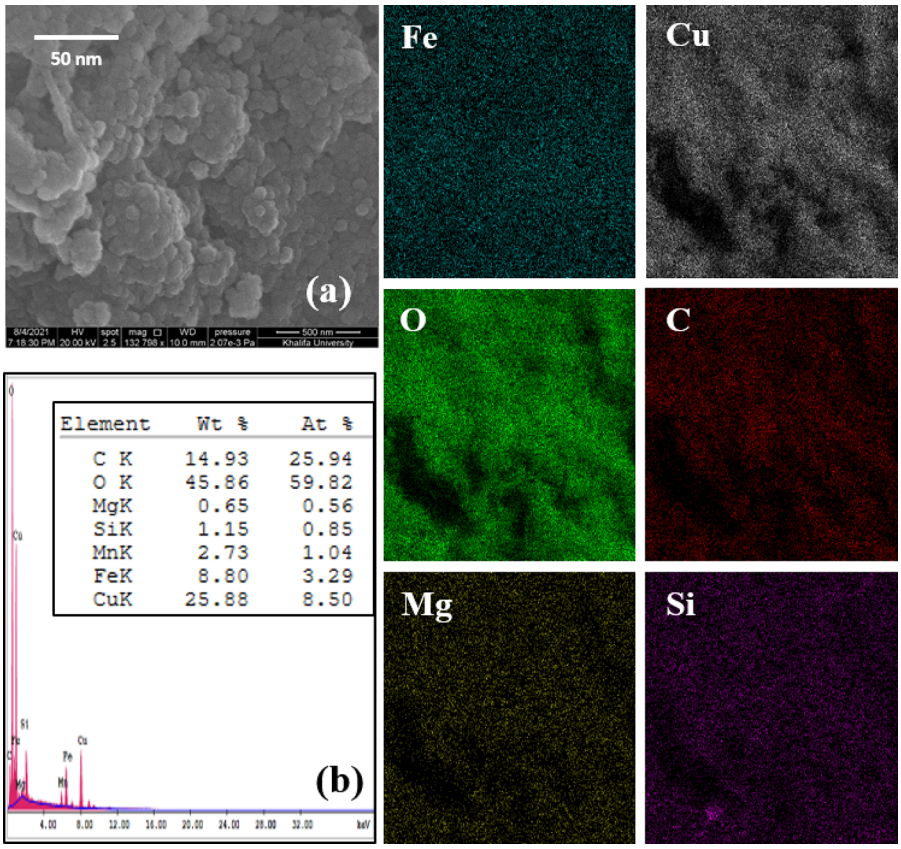


**Figure 3.** (a) SEM and (b) EDX analyses and elemental mapping of CFSG.

assigned to Si−O bonds. The CFSG spectrum shows bands at 971 $cm^{-1}$, which can be assigned to Si−O vibrations, and at 1640 $cm^{-1}$ due to the overlapping of C═C and zeolitic water. The broad band at 400−700 $cm^{-1}$ can be due to the sepiolite bands overlapping with the $CuFe_2O_4$ spinel phase bands (Fe−O at ∼600 $cm^{-1}$ and Cu−O at ∼400−550 $cm^{-1}$).[16,17]

Figure 2a depicts the thermogravimetric analysis of CFSG. Based on the results, the nanocomposite showed its thermal stability up to 700 °C. The first weight loss was observed below 100 °C and can be assigned to the loss of trapped water in the nanocomposite. The second weight loss between 100 and 250 °C involved the pyrolysis of oxygen-containing groups of GO and the loss of zeolitic water.[29] The third weight loss in the range of 250−530 °C can be related to the decomposition of more stable oxygenated functional groups of GO.[30] The DTA graph showed an endothermic peak at 69 °C due to the weight loss in the first dehydration stage.

The XRD analysis (Figure 2b) indicates that the $CuFe_2O_4$ NPs exhibited a cubic crystal phase identified by the diffraction peaks that correspond to the (311), (222), and (400) planes. The lower intensities of these peaks can be attributed to the distorted crystal lattice of the $CuFe_2O_4$ induced by sepiolite and GO.[18,31] The XRD pattern presented in Figure 2b



https://doi.org/10.1021/acsomega.3c02006
ACS Omega 2023, 8, 38828−38838

confirms the cubic phase of the $CuFe_2O_4$ NPs, which agrees with the JCPDS card no. 77-0010.[32,33]

The morphological structure of the CFSG nanocomposite was observed using SEM, as presented in Figure 3a. The nanocomposite possessed a relatively porous structure. In addition, it exhibited quasi-spherical NPs with low agglomeration, which could be attributed to the incorporation of $CuFe_2O_4$ on sepiolite and GO. The EDX results (Figure 3b) of the CFSG nanocomposite confirm the presence of Cu, Fe, C, O, Mg, and Si, while the EDX mapping shows the homogenous distribution of the detected elements in the nanocomposite.

The TEM images of the CFSG composite are presented in Figure 4a,b, which show that sepiolite rods were supported on GO sheets, and quasi-spherical $CuFe_2O_4$ NPs were dispersed on the GO sheets and sepiolite rods. The $CuFe_2O_4$ crystal lattice fringes were clearly observed in the HR-TEM image in Figure 4c. They had d-spacing values of 0.245 and 0.219 nm corresponding to the (311) and (400) crystal planes, respectively,[16,33,34] which is in agreement with the XRD results. Figure 4d shows the selected area electron diffraction (SAED) pattern with the characteristic diffraction pattern of the $CuFe_2O_4$ NPs in which the crystal planes were assigned based on the measured d-spacing values.[35]

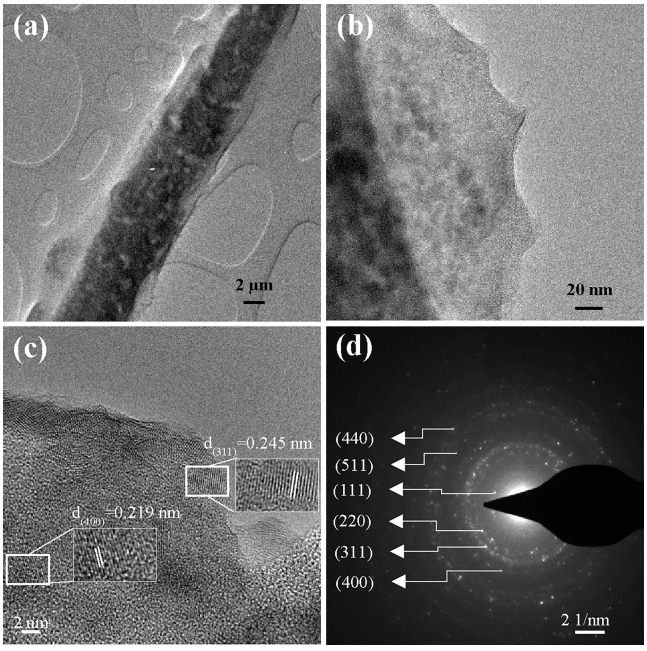


**Figure 4.** (a, b) TEM images at different magnifications, (c) HR-TEM image, and (d) SAED patterns of CFSG.

**3.2. Preliminary Adsorption Studies.** Preliminary adsorption experiments were carried out using GO, sepiolite, $CuFe_2O_4$, and CFSG to investigate the adsorption efficiency of each component. The batch experiments were performed using 10 mg of the adsorbent added to 100 mg/L solution of $Pb(NO_3)_2$ and $CdCl_2{\cdot}2.5H_2O$ at room temperature without any pH modification. The samples were placed in a water bath shaker at 150 rpm for 24 h until equilibrium was established. The samples were collected and filtered using 0.2 $\mu$m nylon filters, and the filtrate was diluted 10 times and analyzed by an inductively coupled plasma optical emission spectrometer (ICP-OES). The adsorption capacity was calculated using the following equation.

$$q_e = \frac{(C_e - C_f)}{m_{(CFSG)}} \times v_{HM} \quad (1)$$

where $q_e$ is the adsorption uptake at equilibrium (mg/g), $m_{(CFSG)}$ is the initial mass of the adsorbent, $v_{HM}$ is the volume of the solution, and $C_e$ and $C_f$ are the initial and final concentrations of Pb(II) and Cd(II), respectively. The adsorption results are presented in Figure 5a, which shows that the adsorption capacity of the adsorbents ranged between 13.83 and 96.48 mg/g for Pb(II) and from 0.21 to 16.27 mg/g for Cd(II). The CFSG nanocomposite exhibited the highest adsorption capacity for both heavy metals compared to the individual components. The $CuFe_2O_4$ uptake alone can be limited due to the agglomeration of the nanoparticles. In the CFSG nanocomposite, $CuFe_2O_4$ nanoparticles were supported on sepiolite and GO, which overcame the problem of agglomeration and facilitated access to $CuFe_2O_4$ adsorption sites, resulting in higher adsorption capacities for CFSG. It is

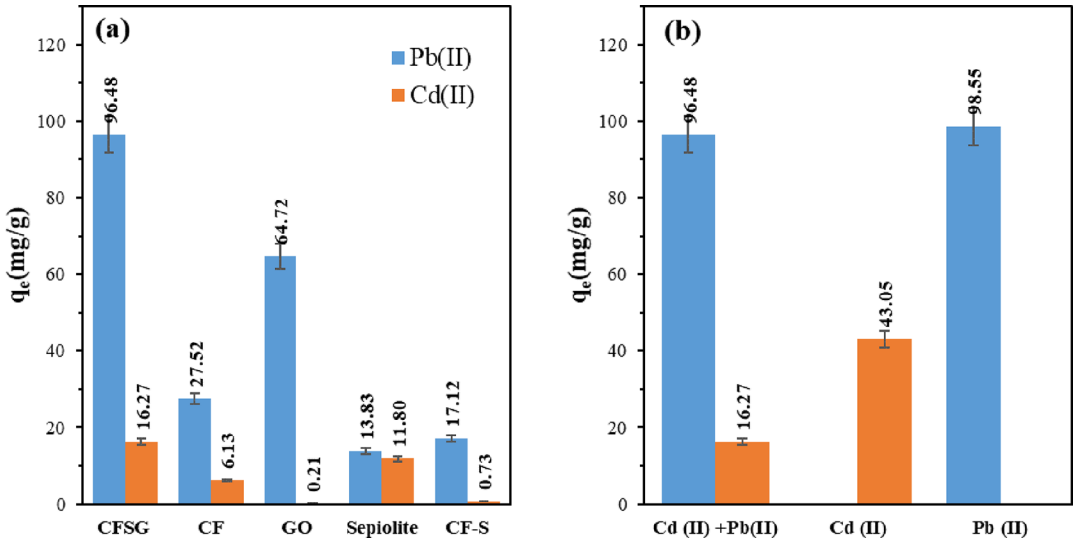


**Figure 5.** (a) Pb(II) and Cd(II) removal screening with different adsorbents and (b) binary and single-metal adsorption on CFSG.



https://doi.org/10.1021/acsomega.3c02006
ACS Omega 2023, 8, 38828−38838

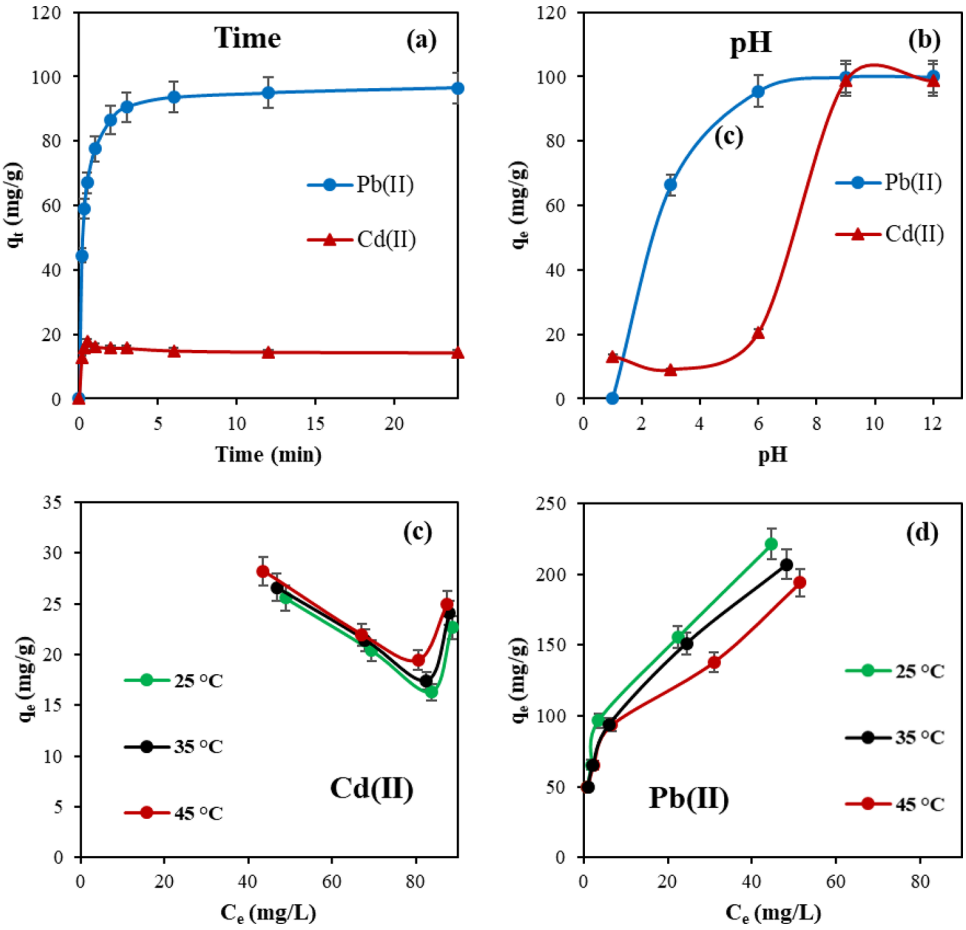


**Figure 6.** Effect of (a) contact time, (b) pH, and temperature on (c) Cd(II) and (d) Pb(II) adsorption.

worth mentioning that the functional groups of the adsorbents (Figure 1) could be related to their adsorption capacities. Therefore, the CFSG nanocomposite with more functional groups is expected to have higher adsorption capacity.[36]

**3.3. Binary and Single Metal Systems.** The presence of more than one heavy metal ion can influence the adsorption process. Therefore, the adsorption of Pb(II) and Cd(II) in both binary and single-metal systems was investigated. Based on the experimental data presented in Figure 5b, the adsorption of each of Pb(II) and Cd(II) in a single-metal system was relatively better than in the binary system. For the Pb(II) case, a slight increase in the adsorption capacity was observed in the single-metal system compared to the binary system whereas Cd(II) adsorption was noticeably higher in the single-ion system. A possible explanation for this is that CFSG favors Pb(II) adsorption over Cd(II) in the binary system.[36] Therefore, once Pb(II) is excluded, i.e., in the single Cd(II) system, the CFSG adsorption sites are solely available for Cd(II). It is worth mentioning that in real wastewater, the coexisting other ions (e.g., $Ca^{2+}$, $Na^{+}$, $Mg^{2+}$) in water would alter the adsorption process as they compete with the adsorbate over the adsorption sites.[37]

*3.3.1. Effect of Contact Time.* The time required to establish adsorption equilibrium was determined by studying the adsorption process at different time intervals. The adsorption studies were conducted for 24 h, and samples were collected periodically and analyzed using ICP-OES. Based on the obtained results in Figure 6a, Pb(II) and Cd(II) showed a fast initial adsorption process within 2 h, but then slowed down until reaching equilibrium. Initially, rapid adsorption occurred due to the abundance of the CFSG adsorption sites, but after that, it slowed down due to the decrease in Pb(II) and Cd(II) concentrations with time and the occupation of the adsorption sites.

*3.3.2. Effect of pH.* The pH is an essential factor in the adsorption process as it directly impacts the interaction between metal ions and the adsorbent. The concentration of protons can influence the speciation of metal ions and alter the adsorbent surface charge and functionality.[38] Figure 6b shows the adsorption of Pb(II) and Cd(II) in the pH range of 1−12. Clearly, a higher percentage of removal was observed in the alkaline medium, which could provide more negatively charged adsorption sites to cationic Pb(II) and Cd(II). In contrast, in the acidic medium at pH values below 6, the surface groups (primarily carboxyl and hydroxyl) undergo protonation, reducing the removal of cationic Pb(II) and Cd(II). Also, the higher concentration of $H^{+}$ ions in an acidic medium inhabits the adsorption process as $H^{+}$ competes with the metal cations over the adsorption sites, which decreases the adsorption efficiency.[39] Thus, the subsequent adsorption experiments were conducted at neutral pH. It is worth mentioning that similar results were reported for other metal ions.[7,9,11]

*3.3.3. Effect of Temperature.* Batch adsorption experiments were performed at 25, 35, and 45 °C to investigate the effect of temperature on the adsorption of Pb(II) and Cd(II). The results are shown in Figure 6c,d. The two heavy metals exhibited different behaviors toward the increase in temper-


https://doi.org/10.1021/acsomega.3c02006
ACS Omega 2023, 8, 38828−38838

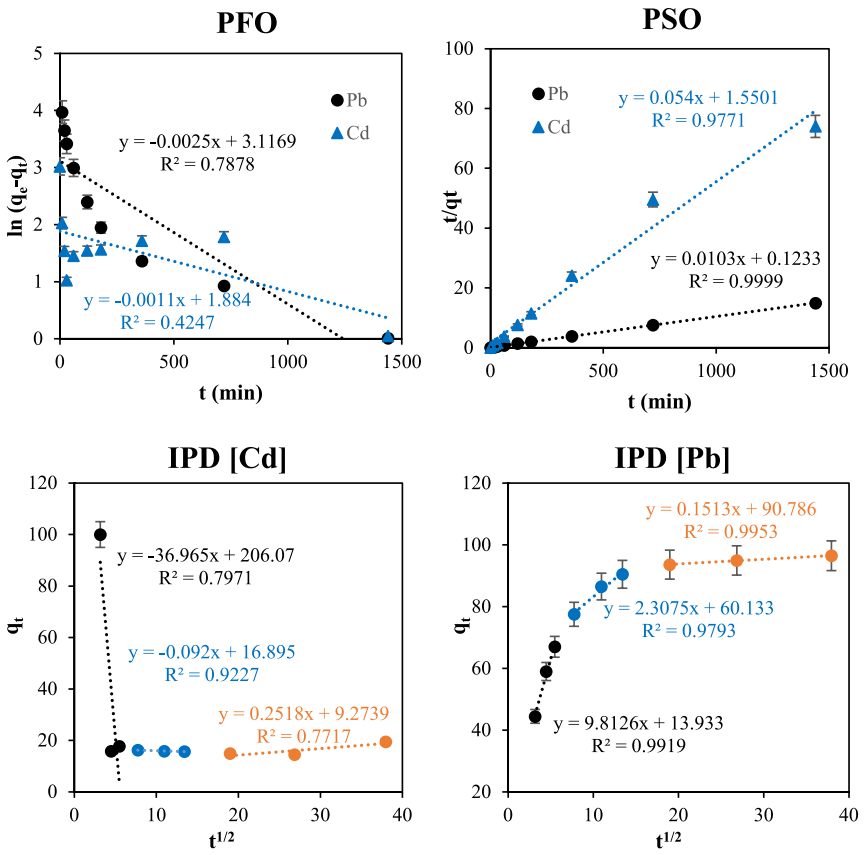


**Figure 7.** Kinetic fitting of the experimental data to PFO, PSO, and IPD for Cd(II) and Pb(II) adsorption.

ature. Pb(II) adsorption decreased with increasing temperature, while Cd(II) adsorption increased. Such adsorption behavior of Pb(II) could be attributed to changes in the electrostatic attraction of Pb(II) to the CFSG surface due to the increased kinetic energy of Pb(II) ions at high temperatures, thus weakening their binding to the CFSG surface. However, the increase in Cd(II) adsorption could be due to the available adsorption sites resulting from Pb(II) desorption at high temperatures. The increase in Cd(II) adsorption at high temperatures could also be due to the increased diffusion rate of the metal ions.

The observed adsorption behavior in Figure 6c could also be related to the CFSG surface inhomogeneity and coadsorption processes. The adsorption of one metal (e.g., Pb(II)) on CFSG increases the complexity of the adsorption surface, and that influences the subsequent adsorption of Cd(II). The observed trend could be the result of nonlinear effects on adsorption capacity caused by changes in solution chemistry or the existence of other competing ions. To fully understand the mechanisms behind this behavior, further experimentation and analysis would be needed.

**3.4. Adsorption Kinetics.** The study of adsorption kinetics is an essential method for understanding the mechanisms of adsorption and identifying the possible controlling step for the rate of the process. The study was conducted at room temperature without any pH modification. Three kinetic models, pseudo-first-order (PFO), pseudo-second-order (PSO), and intra-particle diffusion (IPD), were tested to study Pb(II) and Cd(II) adsorption. The pseudo-first-order model is designed for a physisorption process:

$$\ln(q_e - q_t) = \ln q_e - k_1 t \quad (2)$$

where $q_t$ is the adsorption capacity (mg/g) at a given time ($t$) and $k_1$ is the pseudo-first-order rate constant.

The pseudo-second-order reaction model describes a chemisorption process:

$$\frac{t}{q_t} = \frac{1}{k_2 q_e^2} + \frac{t}{q_e} \quad (3)$$

where $k_2$ is the pseudo-second-order rate constant.

The intra-particle diffusion model analyzes the steps of the adsorption process to determine the rate-controlling step:

$$q_t = k_p t^{1/2} + C \quad (4)$$

where $k_p$ is the intra-particle diffusion rate parameter and $C$ is the coefficient (mg/g).

The three kinetic models were used to model the adsorption data, and the best fitting was estimated based on the linear regression coefficient ($R^2$). The plots of the models are shown in Figure 7, and the kinetic parameters are presented in Table 1. Based on the results, both Pb(II) and Cd(II) adsorption processes were best fitted with the PSO model, confirming that both processes were chemisorption. In addition, the calculated $q_e$ values were very close to the experimental $q_e$ values.

The intra-particle diffusion model showed that both Pb(II) and Cd(II) possessed three adsorption stages that did not pass through the origin point, which indicates that the adsorption was not a diffusion-controlled process. The three adsorption stages are (i) diffusion of Pb(II) and Cd(II) through the mesopores and macropores of the adsorbent (boundary layer);


https://doi.org/10.1021/acsomega.3c02006
ACS Omega 2023, 8, 38828−38838

**Table 1. Comparison of Kinetic Parameters of Various Models for Pb(II) and Cd(II) Adsorption**

| kinetic model | parameters | Pb(II) | Cd(II) |
|---|---|---|---|
| pseudo-first-order | $K_1$ ($min^{-1}$) | 0.0025 | 0.0009 |
| | $R^2$ | 0.7878 | 0.4893 |
| pseudo-second-order | $K_2$ (g/(mg·min)) | 0.000736 | 0.00159 |
| | $R^2$ | 1.00 | 0.9762 |
| | $q_e$ | 97.09 | 18.62 |
| intra-particle diffusion | $K_{d,1}$ ($min^{-1}$) | 9.813 | −36.97 |
| | $R_1^2$ | 0.9919 | 0.7971 |
| | $C_1$ | 13.93 | 206.1 |
| | $K_{d,2}$ ($min^{-1}$) | 2.308 | −0.092 |
| | $R_2^2$ | 0.9793 | 0.9227 |
| | $C_2$ | 60.13 | 16.90 |
| | $K_{d,3}$ ($min^{-1}$) | 0.1513 | 0.2518 |
| | $R_3^2$ | 0.9953 | 0.7717 |
| | $C_3$ | 90.79 | 9.274 |

(ii) diffusion of the adsorbate from mesopores and macropores to micropores; and (iii) sustaining equilibrium.

Each linear region failed to pass through the origin point, indicating that the process was controlled by external mass transfer and diffusion.[7] The boundary diffusion stage was the longest, with a thicker boundary layer indicated by the high $K_{d,1}$ value compared to $K_{d,2}$ and $K_{d,3}$ values. This noticeable difference in values could be due to the mass transfer resistance induced by the heavy metal diffusion into the pores of the adsorbent.[6]

**3.5. Adsorption Isotherms.** The experimental data were fitted using different adsorption models to determine the isotherm that describes the adsorption dynamic. The Langmuir adsorption model implies a monolayer chemisorption process with no adsorbate−adsorbate interaction, and it can be fitted using the following equation:

$$\frac{C_e}{q_e} = \frac{1}{q_{max}K_L} + \frac{C_e}{q_{max}} \quad (5)$$

where $C_e$ is the concentration at equilibrium, $q_e$ is the adsorption uptake at equilibrium, $q_{max}$ is the maximum adsorption capacity for a complete monolayer, and $K_L$ is the Langmuir constant. $R_L$ is a dimensionless separation factor that can be estimated using

$$R_L = \frac{1}{1 + K_L C_0} \quad (6)$$

where $C_0$ is the initial concentration of the heavy metal. The value of $R_L$ provides additional information about the adsorption process. If $R_L > 1$, the process is unfavorable, and if $0 < R_L < 1$, the process is favorable, while $R_L = 0$ describes an irreversible process and $R_L = 1$ describes a linear process.[13]

The Freundlich model describes a multilayer adsorption process on a heterogeneous surface:

$$\log q_e = \log K_F + \frac{1}{n} \times \log C_e \quad (7)$$

where $K_F$ and $n$ are Freundlich's constant and the surface heterogeneity constant, respectively. On the other hand, the Dubinin−Radushkevich (D−R) model draws a clear picture of the nature of the adsorption process, such as its physisorption or chemisorption. The model is expressed using the following equations:

$$\ln q_e = \ln q_{max} - k_D\varepsilon^2 \quad (8)$$

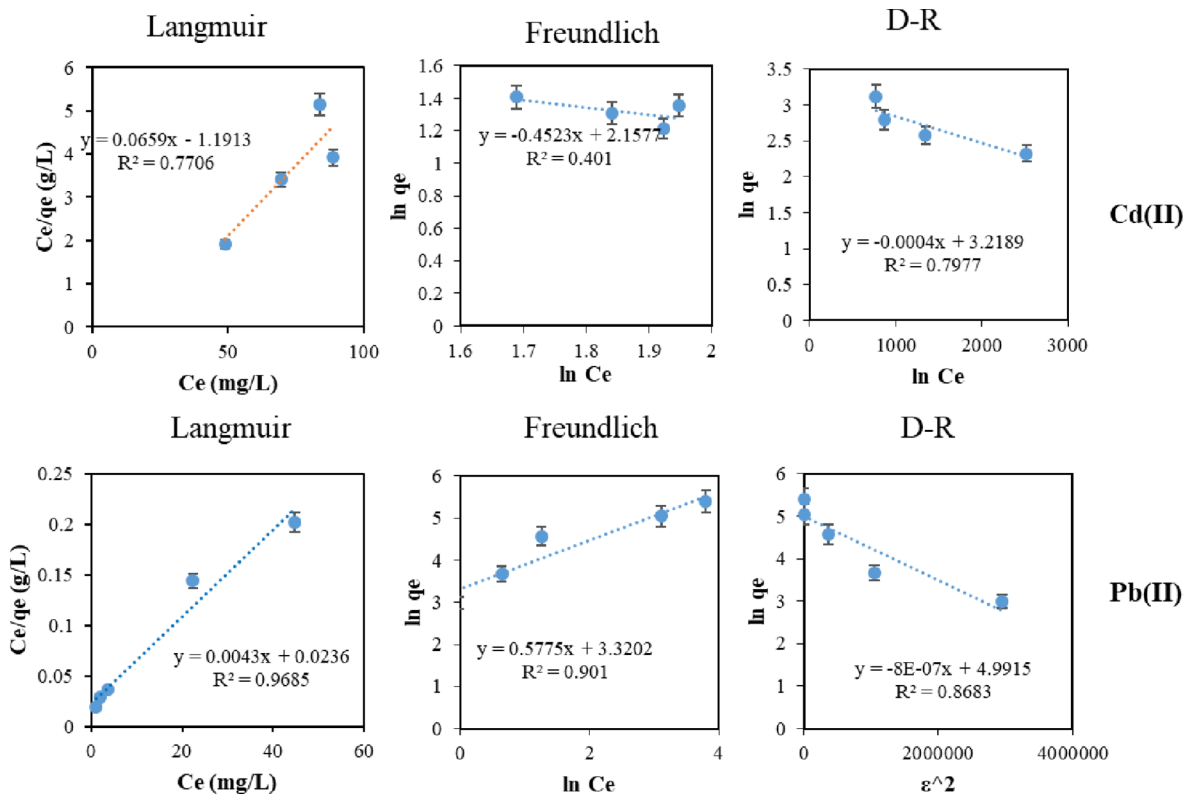


**Figure 8.** Isotherms for Cd(II) and Pb(II) adsorption.



https://doi.org/10.1021/acsomega.3c02006
ACS Omega 2023, 8, 38828−38838

Table 2. Adsorption Isotherm Models and Their Coefficients for Pb(II) and Cd(II) Adsorption

| model | parameter | Cd(II) 25 °C | Cd(II) 35 °C | Cd(II) 45 °C | Pb(II) 25 °C | Pb(II) 35 °C | Pb(II) 45 °C |
|---|---|---|---|---|---|---|---|
| Langmuir | $q_{max}$ (mg/g) | 14.97 | 16.92 | 19.01 | 238.1 | 208.3 | 196.1 |
| | $k_L$ (mg/g) | −0.051 | −0.069 | −0.087 | 0.149 | 0.169 | 0.114 |
| | $R^2$ | 0.7767 | 0.773 | 0.8511 | 0.9622 | 0.9867 | 0.9960 |
| Freundlich | $k_F$ ((mg/g)(L/mg)$^{1/n}$) | 8.815 | 113.8 | 0.1978 | 24.75 | 23.39 | 23.92 |
| | n | −2.179 | −2.571 | 0.9531 | 1.653 | 1.724 | 1.831 |
| | $R^2$ | 0.4168 | 0.3507 | 0.8095 | 0.9642 | 0.9461 | 0.9544 |
| Dubinin−Radushkevich (D−R) | $k_D$ (mol$^2$/kJ$^2$) | $4.00 \times 10^{-4}$ | $3.00 \times 10^{-4}$ | $3.00 \times 10^{-4}$ | $7.00 \times 10^{-7}$ | $8.00 \times 10^{-7}$ | $7.00 \times 10^{-7}$ |
| | $q_{max}$ (mg/g) | 25.00 | 24.23 | 25.10 | 139.0 | 129.6 | 119.3 |
| | $E_S$ (kJ/mol) | 35.36 | 40.82 | 40.82 | 845.2 | 790.6 | 845.2 |
| | $R^2$ | 0.7977 | 0.6433 | 0.6794 | 0.8484 | 0.8462 | 0.7964 |

$$\varepsilon = RT \ln\left(1 + \frac{1}{C_e}\right) \quad (9)$$

$$E_S = \frac{1}{\sqrt{2k_D}} \quad (10)$$

where $k_D$, $\varepsilon$, and $E_S$ (mol$^2$ kJ$^{-2}$) are D−R's activity coefficient (mol$^2$ kJ$^{-2}$), polynali potential, and mean free energy of sorption, respectively.

The adsorption isotherms for Cd(II) and Pb(II) are shown in Figure 8, and the corresponding data are listed in Table 2. For Pb(II), the adsorption process fits well with the Langmuir model based on the correlation values, indicating a chemisorption process that agrees with the previous report on adsorption over $Cu_{0.5}Mg_{0.5}Fe_2O_4$[40] and the previously discussed kinetic study section. Based on the Langmuir model, the maximum Pb(II) adsorption capacity over CFGS was 238.1 mg/g. On the other hand, the fitting of Cd(II) adsorption to Langmuir gave a negative coefficient value and RL > 1, which could be attributed to the decrease in the charge density of the adsorbent due to the increase in the ionic radius of the adsorbate, which hindered the adsorption on the CFSG surface. Therefore, the rapid adsorption of Pb(II) over CFGS increased the ionic radius of the adsorbed layer, resulting in lower adsorption of Cd(II). Table 3 compares the obtained results to the ones reported in the literature. Consequently, CFSG showed a superior uptake in a binary system with evident selectivity toward Pb(II) adsorption.

**3.6. Thermodynamic Study.** Gibbs free energy ($\Delta G°$), the enthalpy change ($\Delta H°$), and the entropy change ($\Delta S°$) thermodynamic parameters for Pb(II) and Cd(II) adsorption were calculated using the following equations:

$$K_c = \frac{q_e}{C_e} \quad (11)$$

$$\Delta G° = -RT \ln k_d \quad (12)$$

$$\ln k_c = \frac{\Delta S°}{R} - \frac{\Delta H°}{RT} \quad (13)$$

where $K_c$ is the equilibrium constant (mg/g), $T$ is the temperature in °K, and $R$ is the universal gas constant 8.314 J/°K·mol. The plot of ln $K_c$ versus $1/T$ determined the thermodynamic parameters, and the results are presented in Table 4. These results provide insight into the changes in energy during the adsorption process and its spontaneity. Therefore, the negative value of $\Delta G°$ for Pb(II) and Cd(II) adsorption indicated that the processes were spontaneous. The Pb(II) adsorption process was exothermic, as shown by the negative value (−18.22 kJ/mol). On the contrary, the positive $\Delta H°$ value (18.17 kJ/mol) for Cd(II) adsorption indicated that it was an endothermic process. However, $\Delta S°$ was positive for both adsorption processes, which means that the adsorption of heavy metal ions was favorable.[44]

Table 3. The Maximum Adsorption Capacity of Pb(II) and Cd(II) Reported for Different Adsorbents

| adsorbent | $q_{max}$ (mg/g) [Pb(II)] | $q_{max}$ (mg/g) [Cd(II)] | ref |
|---|---|---|---|
| green magnesium silicate hydrate | 83.33 | 59.52 | 40 |
| magnetic graphene oxide ($\alpha$-$Fe_2O_3$/GO) | 83.30 | 35.50 | 36 |
| $CoFe_2O_4$-G | 142.8 | 105.3 | 25 |
| $NiFe_2O_4$-G | 111.1 | 74.62 | 25 |
| $NiFe_2O_4$ | 19.88 | 21.53 | 41 |
| CFSG | 238.1 | 14.97 | this work |
| clay honeycomb monoliths (illite−smectite and stevensite) | 1.20 | 4.60 | 42 |
| magnetized activated carbons (rape straw powder) | 253.2 | 73.30 | 43 |

Table 4. Thermodynamic Parameters for Pb(II) and Cd(II) Adsorption on CFSG

| | $T$ (°K) | $\Delta G°$ (kJ/mol) | $\Delta H°$ (kJ/mol) | $\Delta S°$ (kJ/mol·K) |
|---|---|---|---|---|
| Pb(II) | 298 | −36.08 | −18.22 | 60.3 |
| | 308 | −37.10 | | |
| | 318 | −37.27 | | |
| Cd(II) | 298 | −31.57 | 18.17 | 166.7 |
| | 308 | −33.12 | | |
| | 318 | −34.91 | | |

**3.7. Adsorption Mechanism.** The synthesized CFGS adsorbent contains carboxyl (−COO) and hydroxyl (−OH) groups, which serve as adsorption sites and facilitate the removal of heavy metals. SEM−EDX measurements were conducted for the CFSG sample after the adsorption of Pb(II) and Cd(II), as shown in Figure 9a,b. Except for the detection of Pb(II) and Cd(II) after the adsorption, the SEM−EDX results showed no significant changes in the morphological structure or composition of CFSG. Based on the experimental studies, Pb(II) and Cd(II) were removed via the adsorption process on CFSG and a plausible removal mechanism is shown in Figure 9c. As the adsorption was revealed as chemisorption,



https://doi.org/10.1021/acsomega.3c02006
ACS Omega 2023, 8, 38828−38838

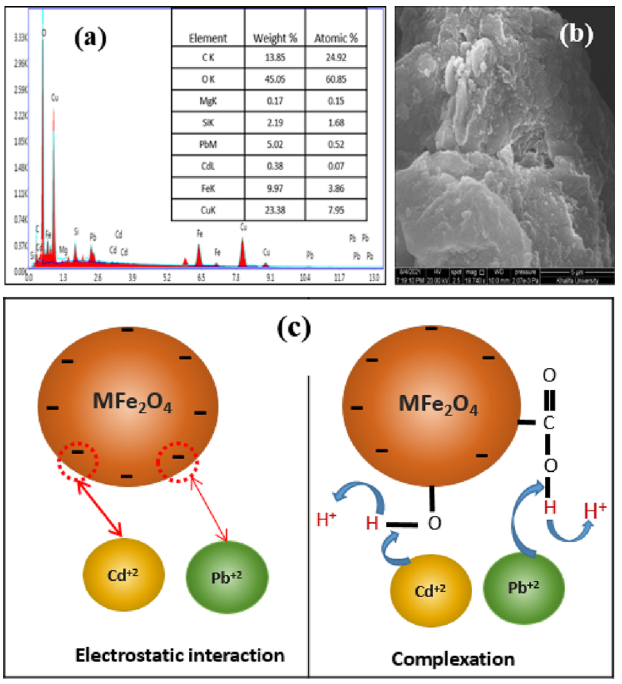


**Figure 9.** (a, b) EDX and SEM of CFSG after Cd(II) and Pb(II) adsorption, and (c) plausible mechanisms of interactions.

it proceeded mainly through electrostatic interactions followed by complex formation with the functional groups on the CFSG surface, which were the main contributors to the adsorption processes.[11] Accordingly, (i) Pb(II) and Cd(II) diffused through the pores of the adsorbent, and then (ii) they adsorbed on the CFSG surface by bonding to the oxygen of the hydroxyl and carboxylic groups of GO and the hydroxyl and silanol groups of sepiolite to form surface complexes (Figure 9c).[45] In addition, the $CuFe_2O_4$ nanoparticles also contributed to the adsorption via the $Fe^{2+}/Fe^{3+}$ redox pair, which donates electrons to heavy metal ions to facilitate their complexation on the CFSG surface.[38,46] Similar observations were reported for Cd(II), Pb(II), and Cu(II) using silica-based nanocomposites and bimetallic Ni/Fe systems, and the removal was attributed to the formation of surface complexes.[10,47]

**3.8. Regeneration Study.** Regeneration conditions, including desorbent (acid, base, salt), shaking time, liquid-to-solid ratio, temperature, and pH, contribute significantly to the adsorption capacity of the recycled adsorbent [50]. As a practical desorbent, the regeneration of CFSG in this work was simply performed with water; the results are presented in Figure 10. The figure shows a decrease in CFSG adsorption capacity after regeneration and reusability. However, it also shows that the CFSG nanocomposite retained more than 70% of its original capacity even after four regeneration cycles using only water. These results can be attributed to the strong chemisorption of Pb(II) or Cd(II), which form stable surface complexes [51].

## 4. CONCLUSIONS

The synthesis of CFSG nanocomposite using a co-precipitation method was reported in this work. The physicochemical properties of CFSG were analyzed using FTIR, SEM−EDX, XRD, TEM, and TGA. The nanocomposite exhibited quasi-spherical $CuFe_2O_4$ nanoparticles supported on sepiolite fibers and GO sheets. The adsorptive removal of Pb(II) and Cd(II) using the CFSG nanocomposite was thoroughly investigated. According to the obtained results, CFSG favored Pb(II) adsorption ($q_m$ = 238.1 mg/g) over Cd(II) ($q_m$ = 14.97 mg/g) in a binary system. The adsorption capacity of the CFSG nanocomposite is higher than the capacities of the individual sepiolite and GO components, which supports the role of $CuFe_2O_4$ in the adsorption process. In addition, the exposed $CuFe_2O_4$ nanoparticles on the surface of CFSG were accessible for interactions with heavy-metal ions, which enhanced the adsorption efficiency. Batch adsorption studies using CFSG were conducted at various experimental conditions, such as pH and temperature, adsorbent loading, and contact time. The isothermal analysis showed that the process was better described using Langmuir for Pb(II) and Cd(II) adsorption. The adsorption processes were spontaneous and followed a pseudo-second-order kinetic for both adsorbates.

## AUTHOR INFORMATION

### Corresponding Author

**Mohammad Abu Haija** − *Department of Chemistry, Khalifa University of Science and Technology, Abu Dhabi 127788, United Arab Emirates; Advanced Materials Chemistry Center (AMCC), Khalifa University of Science and Technology, Abu Dhabi 127788, United Arab Emirates;* orcid.org/0000-0002-5846-0662; Email: mohammad.abuhaija@ku.ac.ae

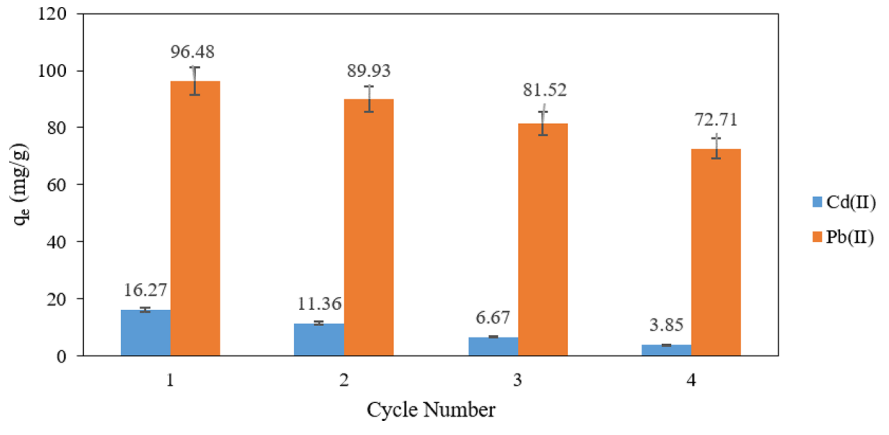


**Figure 10.** Regeneration study of CFGS.



https://doi.org/10.1021/acsomega.3c02006
ACS Omega 2023, 8, 38828−38838

## Authors

**Israa Othman** − *Department of Chemistry, Khalifa University of Science and Technology, Abu Dhabi 127788, United Arab Emirates*

**Fawzi Banat** − *Department of Chemical Engineering and Center for Membranes and Advanced Water Technology (CMAT), Khalifa University of Science and Technology, Abu Dhabi 127788, United Arab Emirates;* orcid.org/0000-0002-7646-5918

**Shadi W. Hasan** − *Department of Chemical Engineering and Center for Membranes and Advanced Water Technology (CMAT), Khalifa University of Science and Technology, Abu Dhabi 127788, United Arab Emirates*

**Cyril Aubry** − *Department of Research Laboratories Operations, Khalifa University of Science and Technology, Abu Dhabi 127788, United Arab Emirates*

**Sundaramurthy Suresh** − *Department of Chemical Engineering, Maulana Azad National Institute of Technology Bhopal, 462003 Bhopal, MP, India*

**Mika Sillanpää** − *Faculty of Environment and Chemical Engineering, Duy Tan University, Da Nang 550000, Vietnam; Department of Chemical Engineering, School of Mining, Metallurgy and Chemical Engineering, University of Johannesburg, Doornfontein 2028, South Africa*

Complete contact information is available at: https://pubs.acs.org/10.1021/acsomega.3c02006


## Notes

The authors declare no competing financial interest.

## ■ ACKNOWLEDGMENTS

The authors acknowledge Khalifa University of Science and Technology for financial support through grant CIRA-2020-85.

## ■ REFERENCES


(1) Saleem, H.; Pal; Haija, M. A.; Banat, F. Regeneration and reuse of bio-surfactant to produce colloidal gas aphrons for heavy metal ions removal using single and multistage cascade flotation. *J. Cleaner Prod.* **2019**, *217*, 493−502.

(2) Desalegn, Y. M.; Andoshe, D. M.; Desissa, T. D. Composite of bentonite/CoFe2O4/hydroxyapatite for adsorption of Pb (II). *Mater. Res. Express* **2020**, *7*, No. 115501.

(3) Okolo, B. I.; Oke, E. O.; Agu, C. M.; Adeyi, O.; Nwoso-Obieogu, K.; Akatobi, K. N. Adsorption of lead(II) from aqueous solution using Africa elemi seed, mucuna shell and oyster shell as adsorbents and optimization using Box−Behnken design. *Appl. Water Sci.* **2020**, *10*, 201.

(4) Tu, Y.-J.; You, C.-F.; Chen, M.-H.; Duan, Y.-P. Efficient removal/recovery of Pb onto environmentally friendly fabricated copper ferrite nanoparticles. *J. Taiwan Inst. Chem. Eng.* **Feb. 2017**, *71*, 197−205.

(5) Guston, D. H. "Institutional Design for Socially Robust Knowledge: The National Toxicology Program's Report on Carcinogens," in *Democratization of Expertise? Exploring Novel Forms of Scientific Advice in Political Decision-Making*, Maasen, S.; Weingart, P. Eds., Dordrecht: Springer Netherlands, 2005, pp. 63−79, DOI: 10.1007/1-4020-3754-6_4.

(6) Edathil, A. A.; Pal, P.; Banat, F. Amine contaminants removal using alginate clay hybrid composites and its effect on foaming. *Int. J. Ind. Chem.* **2019**, *10*, 145−158.

(7) Arshad, F.; Selvaraj, M.; Zain, J.; Banat, F.; Haija, M. A. Polyethylenimine modified graphene oxide hydrogel composite as an efficient adsorbent for heavy metal ions. *Sep. Purif. Technol.* **2019**, *209*, 870−880.

(8) Suresh, S.; Sillanpää, M.; Banat, F.; Vissa, R. K. Adsorption of arsenic in aqueous solution onto iron impregnated bagasse fly ash. *J. Environ. Health Sci. Eng.* **2022**, *20*, 861−879.

(9) Toor, S. K.; Kushwaha, J. P.; Sangal, V. K. Single and Binary Adsorption of Zn (II) and Cr (VI) Heavy Metals onto Synthesized Silica -Based MCM-41. *ChemistrySelect* **2019**, *4*, 2576−2584.

(10) Mahmoud, M. E.; Fekry, N. A.; El-Latif, M. M. A. Nanocomposites of nanosilica-immobilized-nanopolyaniline and crosslinked nanopolyaniline for removal of heavy metals. *Chem. Eng. J.* **2016**, *304*, 679−691.

(11) Singh, S.; Kapoor, D.; Khasnabis, S.; Singh, J.; Ramamurthy, P. C. Mechanism and kinetics of adsorption and removal of heavy metals from wastewater using nanomaterials. *Environ. Chem. Lett.* **2021**, *19*, 2351−2381.

(12) Alqassem, B.; Othman, I.; Abu Haija, M.; Banat, F. Comparative catalytic activity of pure, mixed and P-modified CoFe2O4 nanoparticles for water treatment at neutral pH. *Catal. Commun.* **Feb. 2021**, *150*, No. 106267.

(13) Haija, M. A.; Chamakh, M.; Othman, I.; Banat, F.; Ayesh, A. I. Fabrication of H2S gas sensors using ZnxCu1-xFe2O4 nanoparticles. *Appl. Phys. A: Mater. Sci. Process.* **2020**, *126*, 489.

(14) Haija, M. A.; Ayesh, A. I.; Ahmed, S.; Katsiotis, M. S. Selective hydrogen gas sensor using CuFe2O4 nanoparticle based thin film. *Appl. Surf. Sci.* **2016**, *369*, 443−447.

(15) Kallem, P.; Othman, I.; Ouda, M.; Hasan, S. W.; AlNashef, I.; Banat, F. Polyethersulfone hybrid ultrafiltration membranes fabricated with polydopamine modified ZnFe2O4 nanocomposites: Applications in humic acid removal and oil/water emulsion separation. *Process Saf. Environ. Prot.* **2021**, *148*, 813−824.

(16) Hai, A.; et al. Cobalt and nickel ferrites based capacitive deionization electrode materials for water desalination applications. *Electrochim. Acta* **2020**, *363*, No. 137083.

(17) Othman, I.; Abu Haija, M.; Kannan, P.; Banat, F. Adsorptive Removal of Methylene Blue from Water Using High-Performance Alginate-Based Beads. *Water, Air, Soil Pollut.* **2020**, *231*, 396.

(18) Othman, I.; Abu Haija, M.; Ismail, I.; Zain, J. H.; Banat, F. Preparation and catalytic performance of CuFe2O4 nanoparticles supported on reduced graphene oxide (CuFe2O4/rGO) for phenol degradation. *Mater. Chem. Phys.* **2019**, *238*, No. 121931.

(19) Liu, D.; Wang, C.; Song, Y.; Wei, Y.; He, L.; Lan, B.; He, X.; Wang, J. Effective mineralization of quinoline and bio-treated coking wastewater by catalytic ozonation using $CuFe_2O_4$/Sepiolite catalyst: Efficiency and mechanism. *Chemosphere* **2019**, *227*, 647−656.

(20) Kahangi, F. G.; Mehrdad, M.; Heravi, M. M.; Sadjadi, S. Bio-assisted synthesized Ag(0) nanoparticles stabilized on hybrid of sepiolite and chitin: efficient catalytic system for xanthene synthesis. *Sci. Rep.* **2020**, *10*, 15285.

(21) Banat, F.; Al-Asheh, S.; Abu-Aitah, L. Examination of the Effectiveness of Physical and Chemical Activation of Natural Bentonite for the Removal of Heavy Metal Ions from Aqueous Solutions. *Adsorpt. Sci. Technol.* **2002**, *20*, 151−167.

(22) Gaber, S.; Abu Haija, M.; Priyabrata, P.; Selvaraj, M.; Banat, F. Removal of iron from industrial lean methyldiethanolamine solvent by adsorption on sepiolite. *Sep. Sci. Technol.* **2018**, *53*, 404−416.

(23) Gaber, D.; Abu Haija, M.; Eskhan, A.; Banat, F. Graphene as an Efficient and Reusable Adsorbent Compared to Activated Carbons for the Removal of Phenol from Aqueous Solutions. *Water, Air, Soil Pollut.* **2017**, *228*, 320.

(24) Lan Huong, P. T.; et al. Functional manganese ferrite/graphene oxide nanocomposites: effects of graphene oxide on the adsorption mechanisms of organic MB dye and inorganic As(v) ions from aqueous solution. *RSC Adv.* **2018**, *8*, 12376−12389.

(25) Santhosh, C.; Kollu, P.; Felix, S.; Velmurugan, V.; Jeong, S. K.; Grace, A. N. $CoFe_2O_4$ and $NiFe_2O_4$@graphene adsorbents for heavy metal ions − kinetic and thermodynamic analysis. *RSC Adv.* **2015**, *5*, 28965−28972.

(26) Bharath, G.; Madhu, R.; Chen, S.-M.; Veeramani, V.; Mangalaraj, D.; Ponpandian, N. Solvent-free mechanochemical synthesis of graphene oxide and Fe3O4−reduced graphene oxide

nanocomposites for sensitive detection of nitrite. *J. Mater. Chem. A* **2015**, *3*, 15529−15539.
(27) Othman, I.; Abu Haija, M.; Banat, F. Catalytic Properties of Phosphate-Coated CuFe2O4 Nanoparticles for Phenol Degradation. *J. Nanomater.* **2019**, *2019*, 3698326.
(28) Khoshnam, M.; Farahbakhsh, J.; Zargar, M.; Mohammad, A. W.; Benamor, A.; Ang, W. L.; Mahmoudi, E. $\alpha$-Fe2O3/graphene oxide powder and thin film nanocomposites as peculiar photocatalysts for dye removal from wastewater. *Sci. Rep.* **2021**, *11*, 20378.
(29) Zahirifar, J.; Karimi-Sabet, J.; ali Moosavian, S. M.; Hadi, A.; Khadiv-Parsi, P. Fabrication of a novel octadecylamine functionalized graphene oxide/PVDF dual-layer flat sheet membrane for desalination via air gap membrane distillation. *Desalination* **2018**, *428*, 227−239.
(30) Tene, T.; Tubon Usca, G.; Guevara, M.; Molina, R.; Veltri, F.; Arias, M.; Caputi, L. S.; Vacacela Gomez, C. Toward Large-Scale Production of Oxidized Graphene. *Nanomaterials* **2020**, *10*, 279.
(31) Liu, B.; Wang, W.; Wang, J.; Zhang, Y.; Xu, K.; Zhao, F. Preparation and catalytic activities of CuFe2O4 nanoparticles assembled with graphene oxide for RDX thermal decomposition. *J. Nanopart. Res.* **2019**, *21*, 48.
(32) Caddeo, F.; Loche, D.; Casula, M. F.; Corrias, A. Evidence of a cubic iron sub-lattice in t-CuFe2O4 demonstrated by X-ray Absorption Fine Structure. *Sci. Rep.* **2018**, *8*, 797.
(33) Ahmad Abuilaiwi, F.; Awais, M.; Qazi, U. Y.; Afzal, A. "*Al3+ doping reduces the electron/hole recombination in photoluminescent copper ferrite (CuFe2−xAlxO4) nanocrystallites*," Boletín de la Sociedad Española de Cerámica y Vidrio, 2020, DOI: 10.1016/j.bsecv.2020.11.007.
(34) Kharisov, B. I.; Dias, H. V. R.; Kharissova, O. V. Mini-review: Ferrite nanoparticles in the catalysis. *Arabian J. Chem.* **2019**, *12*, 1234−1246.
(35) Desai, I.; Nadagouda, M. N.; Elovitz, M.; Mills, M.; Boulanger, B. Synthesis and characterization of magnetic manganese ferrites. *Mater. Sci. Energy Technol.* **2019**, *2*, 150−160.
(36) Kadari, M.; Makhlouf, M.; Khaoua, O. O.; Kesraoui, M.; Bouriche, S.; Benmaamar, Z. The Removal Efficiency of Cadmium (Cd2+) and Lead (Pb2+) from Aqueous Solution by Graphene Oxide (GO) and Magnetic Graphene Oxide ($\alpha$-Fe2O3/GO). *Chemistry Africa* **2023**, *6*, 1515.
(37) Dev, V. V.; Nair, K. K.; Baburaj, G.; Krishnan, K. A. Pushing the boundaries of heavy metal adsorption: A commentary on strategies to improve adsorption efficiency and modulate process mechanisms. *Colloid Interface Sci. Commun.* **2022**, *49*, No. 100626.
(38) Al Yaqoob, K.; Bououdina, M.; Akhter, M. S.; Al Najar, B.; Vijaya, J. J. Selectivity and efficient Pb and Cd ions removal by magnetic MFe2O4 (M=Co, Ni, Cu and Zn) nanoparticles. *Mater. Chem. Phys.* **2019**, *232*, 254−264.
(39) Tran, C. V.; Quang, D. V.; Nguyen Thi, H. P.; Truong, T. N.; La, D. D. Effective Removal of Pb(II) from Aqueous Media by a New Design of Cu-Mg Binary Ferrite. *ACS Omega* **2020**, *5*, 7298−7306.
(40) Qing, Z.; Guijian, L.; Shuchuan, P.; Chuncai, Z. The simultaneous removal of cadmium (II) and lead (II) from wastewater with the application of green synthesized magnesium silicate hydrate. *Front. Earth Sci.* **2023**, *10*, 1074687.
(41) Khoso, W. A.; Haleem, N.; Baig, M. A.; Jamal, Y. Synthesis, characterization and heavy metal removal efficiency of nickel ferrite nanoparticles (NFN's). *Sci. Rep.* **2021**, *11*, 3790.
(42) Ahrouch, M.; Gatica, J. M.; Draoui, K.; Bellido-Milla, D.; Vidal, H. Clay honeycomb monoliths for the simultaneous retention of lead and cadmium in water. *Environ. Technol. Innovation* **2022**, *27*, No. 102765.
(43) Zhang, Z.; Wang, T.; Zhang, H.; Liu, Y.; Xing, B. Adsorption of Pb(II) and Cd(II) by magnetic activated carbon and its mechanism. *Sci. Total Environ.* **2021**, *757*, No. 143910.
(44) Yahya, M. D.; Aliyu, A. S.; Obayomi, K. S.; Olugbenga, A. G.; Abdullahi, U. B. Column adsorption study for the removal of chromium and manganese ions from electroplating wastewater using cashew nutshell adsorbent. *Cogent Eng.* **2020**, *7*, 1748470.
(45) A., Çetinkaya; S., Özçakmak "*Specification of Mineral Composition, Heavy Metal Content, Microbiological Characteristics of a Traditional Anatolian Cheese-Aho Cheese*," 2018, DOI: 10.21276/sb.2017.3.12.5.
(46) Fu, F.; Wang, Q. Removal of heavy metal ions from wastewaters: a review. *J. Environ. Manage.* **2011**, *92*, 407−418.
(47) Cai, X.; Gao, Y.; Sun, Q.; Chen, Z.; Megharaj, M.; Naidu, R. Removal of co-contaminants Cu (II) and nitrate from aqueous solution using kaolin-Fe/Ni nanoparticles. *Chem. Eng. J.* **2014**, *244*, 19−26.


https://doi.org/10.1021/acsomega.3c02006
*ACS Omega* 2023, 8, 38828−38838